Q. J. R. Meteorol. Soc. (2005), **131**, pp. 109–124 doi: 10.1256/qj.03.163

On type B cyclogenesis in a quasi-geostrophic model

By RICHARD GROTJAHN*
University of California, Davis, USA

(Received 22 September 2003; revised 24 August 2004)

SUMMARY

A quasi-geostrophic (QG) model is used to approximate some aspects of 'type B' cyclogenesis as described in an observational paper that appeared several decades earlier in this journal. Though often cited, that earlier work has some ambiguity that has propagated into subsequent analyses. The novel aspects examined here include allowing advective nonlinearity to distort and amplify structures that are quasi-coherent and nearly stable in a linear form of the model; also, separate upper and lower structures are localized in space. Cases are studied separately where the upper trough tracks across different low-level features: an enhanced baroclinic zone (stronger horizontal temperature gradient) or a region of augmented temperature. Growth by superposition of lower and upper features is excluded by experimental design. The dynamics are evaluated with the vertical motion equation, the QG vorticity equation, the QG perturbation energy equation, and 'potential-vorticity thinking'. Results are compared against 'control' cases having no additional low-level features. Nonlinearity is examined relative to a corresponding linear calculation and is generally positive. The results are perhaps richer than the seminal article might imply, because growth is enhanced not only when properties of the lower feature reinforce growth but also when the lower feature opposes decay of the upper feature. For example, growth is enhanced where low-level warm advection introduces rising warm air to oppose the rising cold air ahead of the upper trough. Such growth is magnified when adjacent warm and cold anomalies have a strong baroclinic zone between them. The enhanced growth triggers an upstream tilt in the solution whose properties further accelerate the growth.

KEYWORDS: Baroclinic instability Nonlinear instability Quasi-geostrophic dynamics

1. INTRODUCTION

A search of the Science Citation Index for the period 1975 to early 2004 finds 165 citations of Petterssen and Smebye (1971; hereafter P&S). Most of the articles that cite P&S are case-studies of specific events, such as particularly severe frontal cyclones. Some articles refer to the extensive kinetic energy (KE) analyses P&S undertake for two developing frontal cyclones. Other articles describe results from idealized theoretical constructs based to varying degrees on the 'type B' conceptual model introduced by P&S. The present note relates to the latter association and is a novel test of the type B construct in an idealized theoretical model.

P&S attempt to place observed cyclogenesis into two categories, one of which is labelled type B. They list a sequence of events in a table that emphasizes low-level warm advection: 'Development commences when a pre-existing upper trough, with strong vorticity advection on its forward side, spreads over a low-level area of warm advection . . . '.

However, in their later discussion, they emphasize 'baroclinicity', which is left undefined but appears to be qualitatively proportional to the horizontal gradient of 850–500 hPa thickness since that field is shown and discussed by P&S. (They also use baroclinicity in reference to KE increasing with height.) Further, their quantitative analysis emphasizes the KE equation in which warm advection does not explicitly appear. However, warm advection might be viewed as leading to upward motion (they discuss a vertical motion diagnostic equation) and vertical motion appears in a couple of terms in their KE equation. Upward moving relatively warmer air (and/or sinking air of relatively higher density) might be thought to increase KE by lowering the centre of mass for the storm as a whole (thereby converting potential energy into KE).

* Corresponding address: Department of Land, Air and Water Resources, University of California, Davis, CA 95616, USA. e-mail: grotjahn@ucdavis.edu

They show values of terms in the KE equation integrated over a very large area that extends well beyond each developing cyclone. They do not explicitly show a warm-advection contribution. This inconsistency may explain why later works by others stray from the original descriptions in P&S.

Theoretical studies have had various interpretations of type B cyclogenesis. Farrel (1984) examined initial-value problems with a single trough extending from surface to model top and tilted against the shear. However, P&S appear to be describing separate upper and lower features, such as are commonly observed (Grotjahn 1996a) prior to cyclogenesis. Also P&S refer to a lower baroclinic zone, not a surface trough *per se*. Whitaker and Barcilon (1992) use a channel model, with a middle portion in the along-flow direction having greater baroclinic instability (due to a combination of lowered static stability, higher vertical shear in the lower troposphere, and less Ekman damping). Whitaker and Barcilon then send an upper-level packet of waves towards their region of higher baroclinicity. Other studies have considered localized wave packets (e.g. Swanson and Pierrehumbert 1994). However, P&S probably envisaged a single trough, not a dispersing packet of troughs and ridges. Other studies have considered an initially isolated trough (e.g. Hakim 2000). However, studies like Hakim (2000) and Rotunno and Bao (1996) use initial conditions that are inherently unstable; the solutions develop immediately and do not wait until an approximately neutral upper trough encounters a 'low-level baroclinic zone'. Mitsudera (1994) created interaction between upper- and lower-level solitary waves, and interpreted the resulting development in the type B context, though it is unclear how the lower solitary wave models a surface baroclinic zone. These and other studies of localized structures are discussed further in Grotjahn *et al.* (2003).

The present work focuses rather narrowly on casting a theoretical model to match more closely the type B cyclogenesis mechanism envisioned by P&S. After discussing several formulations of the model, some results are summarized and interpreted using standard tools.

2. Experimental set-up

The type B theoretical construct here attempts to improve upon some aspects of earlier constructions mentioned above. The model is three-dimensional (not two-layer). The upper feature extends through much of the upper troposphere and consists of a single trough (not a wave-train; Fig. 1); it is nearly stable (not linearly unstable). Normal-mode growth is excluded from the linear set-up. The upper feature is nearly coherent (in a linear calculation). Non-modal growth, to the extent that it depends on phase-speed differences of eigenmode constituents is very small. Hence, changes seen are essentially due to type B interaction. The surface baroclinic zone is at least partly oriented across the path of the upper trough, as might occur when a surface front lies across the path of an upper trough. While the intent of the model is to improve upon type B simulations, the model still has major limitations: it is quasi-geostrophic (QG), adiabatic, and uses Cartesian geometry.

The model is fully described in Grotjahn *et al.* (2003) and Grotjahn (1980). The nonlinear form of the interior QG potential vorticity (PV) equation used here is:

$$\frac{\partial q}{\partial t} + \mathrm{J}(\overline{\Psi}_1 + \overline{\Psi}_2, q) + \mathrm{J}(\psi, Q_1 + Q_2) + \mathrm{J}(\psi, q) = 0, \tag{1}$$

where J denotes a Jacobian; other upper-case variables, and variables with overbars, are specified, fixed, and form the prescribed state; t is time, and ψ is the perturbation stream function. Subscript 1 refers to the zonal mean flow basic state; subscript 2 refers

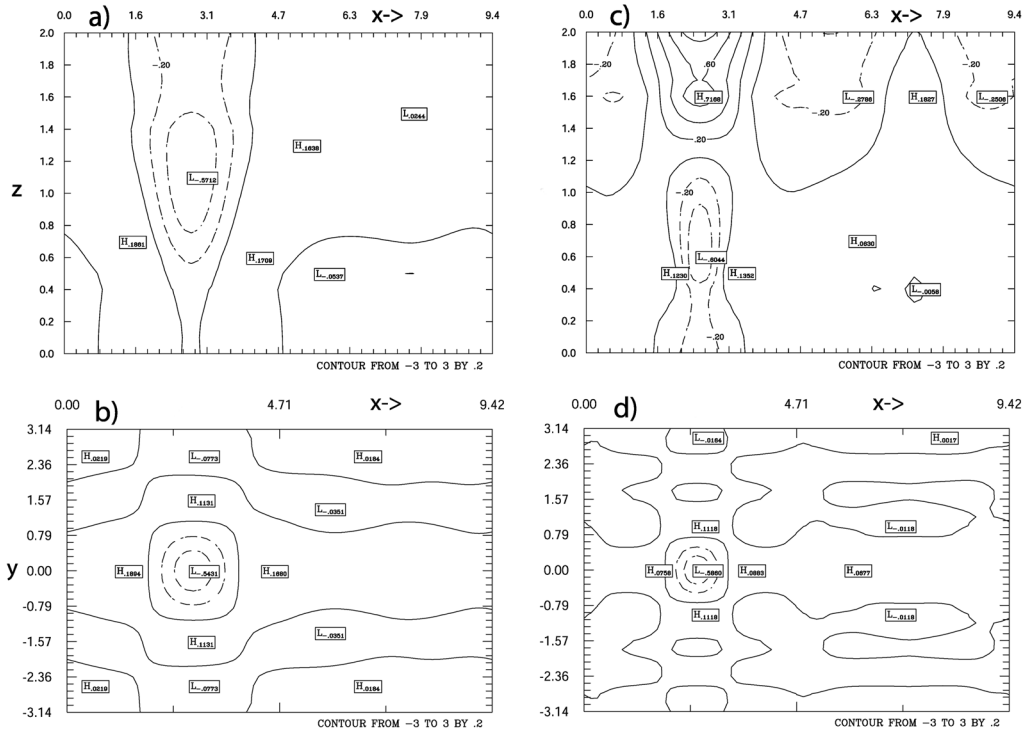

Figure 1. Nearly coherent upper troughs constructed from neutral eigenmodes and used as an initial condition (IC). 'Deep' IC shown in: (a) zonal cross-section at $y = 0$, and (b) horizontal plane at $z = 0.9$. 'Mid8' IC shown in: (c) zonal cross-section at $y = 0$, and (d) horizontal plane at $z = 0.8$. The Deep IC is used for horizontally uniform basic flows, and the mid8 IC is used for a Bickley jet basic flow. All fields shown are non-dimensional. See text for details.

to a three-dimensionally varying surface feature when it is prescribed. The perturbation QGPV is:

$$q = \nabla^2\psi + \frac{1}{\rho}\frac{\partial}{\partial z}\left(\rho\varepsilon\frac{\partial\psi}{\partial z}\right). \tag{2}$$

The boundary conditions in the vertical are:

$$\frac{\partial}{\partial t}\left(\frac{\partial\psi}{\partial z}\right) + \mathrm{J}\left(\overline{\Psi}_1 + \overline{\Psi}_2,\ \frac{\partial\psi}{\partial z}\right) + \mathrm{J}\left(\psi,\ \frac{\partial\overline{\Psi}_1}{\partial z} + \frac{\partial\overline{\Psi}_2}{\partial z}\right) + \mathrm{J}\left(\psi,\ \frac{\partial\psi}{\partial z}\right) = 0 \quad \text{at } z = 0,\ z_{\text{top}} \tag{3}$$

where z_{top} is the top of the model atmosphere. The equations are made non-dimensional by using typical scaling magnitudes for horizontal length ($L = 1000$ km), vertical depth ($D = 10$ km), speed ($V = 10$ m s^{-1}), and advective time scale ($L/V = 10^5$ s). Parameter $\varepsilon = \{f_0 L/(ND)\}^2$, relates L to the Rossby radius of deformation, and so is inversely proportional to Brunt–Väisälä frequency, N. Density, ρ, and static stability are functions of z only and are chosen to match the US Standard Atmosphere (1976) midlatitude profiles (Grotjahn (1980) gives further details). The model uses Cartesian coordinates on a midlatitude 'β-plane' channel having linear Coriolis variation. Initial-value calculations are performed using linear and nonlinear forms of this model. The linear form does not have the third Jacobian in (1) and (3). The initial-value problem is solved numerically using: Adams–Bashforth time differencing, spectral formulation

in the horizontal (11 wave numbers in x and 10 in y), and centred vertical differences (21 layers from $0 \leqslant z \leqslant 2$).

The basic state zonal wind (U_1) and $\partial Q_1/\partial y$ can be functions of z and y. The basic wind vertical profile reaches its maximum value at the tropopause ($z = 1.0$; 10 km) and decreases with height in the model's stratosphere. Two horizontal specifications are tested: no horizontal shear with peak U_1 value of 1.2 (12 m s^{-1}), and a Bickley jet with peak U_1 value of 3.6 units (36 m s^{-1}). The basic flow with no horizontal shear uses the basic state stream function $\overline{\Psi}_1 = -yU_1$, while the Bickley jet uses $\overline{\Psi}_1 = -3\tanh(y)U_1$. The no-horizontal-shear flow allows comparison to our past works (e.g. Grotjahn 1984; Hodyss and Grotjahn 2003 and references therein). The Bickley jet reaches a more realistic magnitude.

Eight different model configurations result from these three pairs of combinations: (i) nonlinear or linear formulations, (ii) a low-level feature evolves or is kept fixed as part of the prescribed state, and (iii) no horizontal shear or a Bickley jet.

The upper feature is carefully constructed from neutral eigenmodes having very similar phase speed. The lower feature is constructed similarly when it is allowed to evolve. The result is a feature that is nearly coherent for a linear calculation. The coherent upper trough simulates observed cyclone precursors (Grotjahn 1996a), wherein an upper-level trough is localized (i.e. not part of a wave-train; Grotjahn and Castello (2000)) and is approximately neutral until it encounters a surface feature that initiates cyclogenesis. Two upper troughs are tested here. One upper trough has little amplitude below 3 km, similar to observed cyclogenesis precursor troughs (Grotjahn, 1996a); see Figs. 1(a) and (b). This trough is referred to as the 'deep' initial condition (IC) in Grotjahn *et al.* (2003) and that nomenclature is retained here. This IC is constructed from eigenmodes from the basic flow without horizontal shear. The other upper trough has a primary maximum in the upper troposphere and a secondary maximum near the surface; (see Figs. 1(c) and (d)) This IC is referred to as the 'mid8' IC here and in Grotjahn *et al.* (2003). Eigenmodes used to construct the mid8 IC come from the analysis of a strong, internal Bickley jet basic flow.

Similar to the initial upper trough, the low-level feature (e.g. surface baroclinic zone) should be coherent and nearly neutral prior to favourable alignment with the upper trough. 'Favourable alignment' refers to one or more places along the path followed by the upper trough where the development of the upper trough is enhanced by properties of the surface feature. Two approaches can accomplish this: one is to construct the surface feature from shallow, surface-trapped, very slow moving neutral eigenmodes; the other is to use a formula (if not a sum of eigenmodes) to specify a surface feature that is included in the *prescribed* state. The second approach has the advantage of removing changes to the upper trough that might arise from superposition upon the surface feature. Such superposition is hard to exclude using the first approach, because the surface feature will evolve (albeit slowly) and has amplitude (though initially small) at all levels; these properties are sufficient to obscure the type B mechanism. When the prescribed flow contains the low-level feature, superposition is excluded. However, the second approach allows the upper feature to react to the lower, but they do not interact.

P&S refer to temperature advection and to a baroclinic zone at low levels. In the QG framework a vertical derivative of stream function is proportional to potential temperature. So, each low-level feature has an associated perturbation-temperature field. The strength of the low-level temperature perturbations can be judged from Fig. 2. Four types of surface features are examined depending on the sign of the feature and whether it is a monopole (as in Fig. 2(a)) or a dipole (as in Fig. 2(b)). The monopole

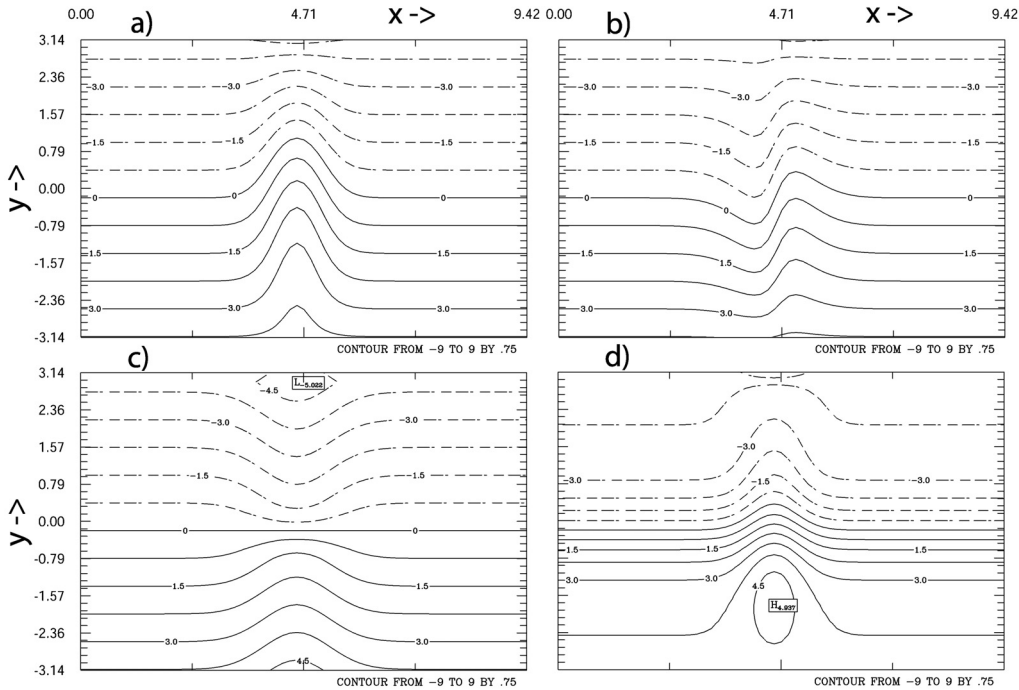

Figure 2. Examples of localized low-level features in the total prescribed surface temperature field: (a) 'warm' monopole, (b) 'cold-front' dipole, and (c) 'warm-front' dipole perturbations for the horizontally uniform basic flow; (d) 'warm' monopole for the Bickley jet basic flow. Fields shown are non-dimensional.

pattern is either a pocket of warm air or a pocket of cold air. The 'warm monopole' (Fig. 2(a)) is a surface trough that decreases in amplitude with increasing height, hence it is also a positive maximum in QGPV. The 'cold monopole' has opposite sign. A dipole pattern allows a concentration of the isentropes in the middle that crudely models a frontal zone. The type B mechanism is sometimes portrayed as an upper trough approaching a surface cold front. To address this situation a 'cold-front' case is considered, wherein a cold anomaly is west of a warm anomaly (Fig. 2(b)). When not prescribed, the cold-front case has enhanced *cold* advection in the middle of the low-level feature. The opposite dipole orientation, where the warm air pocket is west of the cold air pocket, is uncommon. Instead, we place a warm anomaly south of a cold anomaly, leading to a local enhancement of the meridional temperature gradient; this case is labelled the 'warm-front' case (Fig. 2(c)). (These names are indicative and not technically precise: a real warm front moves but in this model it does not; the cold front only moves when allowed to evolve in this model.)

Warm and cold anomalies can be constructed either from analytic functions or from neutral eigenmodes. When the entire IC is comprised of neutral eigenmodes, these modes do not interact in a linear calculation and there is no exponential growth. The other possibility: non-modal growth (NG) by increasing reinforcement of constituent modes is very small, since the constituents of each feature have very similar phase speeds. NG is not zero because the phase speeds are not identical. For no-horizontal-shear cases, the upper and lower features have little overlap in amplitude; thus, even though the upper and lower features move at different speeds,

NG is still small. The upper trough tends to slowly loose its coherence in a linear calculation, making the upper-level growth rate small and negative. When the surface feature is placed in the prescribed state, the neutral modes used to construct the upper feature are no longer true eigenmodes to the problem, and that allows the upper trough to grow or decay, even in a linear calculation, once some portion of the upper trough encounters the surface feature.

Adding nonlinearity to the horizontal advection terms initiates additional eigenmodes, including exponentially growing (and possibly decaying) modes. These normal modes and other neutral modes have different phase speeds, and that accelerates the dispersion. Grotjahn *et al.* 2003, find a remarkably small number (three to six) of the normal modes and one neutral mode to be prominently activated for the IC and basic flows used here. The nonlinearity disrupts the linear coherency of the features, which somewhat obscures the growth-rate changes being sought. To mitigate against such issues, results are shown in comparison to a control. The control is an analogous calculation but without the low-level feature. The differences between linear and nonlinear solutions also isolate the nature of the changes.

Another issue requiring care is the method used to measure growth. The features are localized, and a global measure of growth (such as the eddy KE within the whole domain) can be ambiguous if not misleading. (P&S appear to track KE in a domain much larger than each storm in their study.) Selecting a domain that encompasses just the perturbation is ultimately ambiguous, made more so when the scale of the feature changes over time, and the domain is arguably different at different levels. This issue is discussed further in Grotjahn *et al.* (2003). Growth here is measured by tracking the peak value of the feature over time. Since the structure also changes over time, the peak value is tracked at more than one level.

3. Selected results

(*a*) *General properties*

The preceding section discusses the considerable care taken in the experimental design. If such care is not taken the results can be misleading. Choosing an *arbitrary* localized structure for the IC and allowing it to evolve (instead of a carefully balanced trough such as that from summing carefully chosen eigenmodes) will lead to rapid growth of structures like normal modes, while simultaneous (possibly rapid) dispersion occurs. Starting adjacent to the isolated features, more and more troughs and ridges appear until they fill the domain. (In a linear calculation the most unstable mode eventually dominates.) Growth of an arbitrary initial feature is not associated with any particular 'favourable' alignment between upper and lower feature, and is clearly not type B development.

Figure 3 illustrates the point by comparing integrations using an IC combining the deep upper trough with a low-level, analytic, cold monopole, against integrations having an IC with just the cold monopole. The deep IC alone (not shown) is nearly balanced; it has approximate coherence and slow decay by dispersion. At first glance the combination of deep IC and analytic cold monopole appears to show growth commencing once the upper trough arrives at the cold monopole. While this may look like type B growth, the apparently favourable alignment is fortuitous superposition. Figure 3(f) shows the corresponding solution when the IC is solely the analytic cold monopole; the pattern is very similar to the combination (see Fig. 3(e)). The analytic function decomposes into a suite of eigenmodes, including those having different speeds

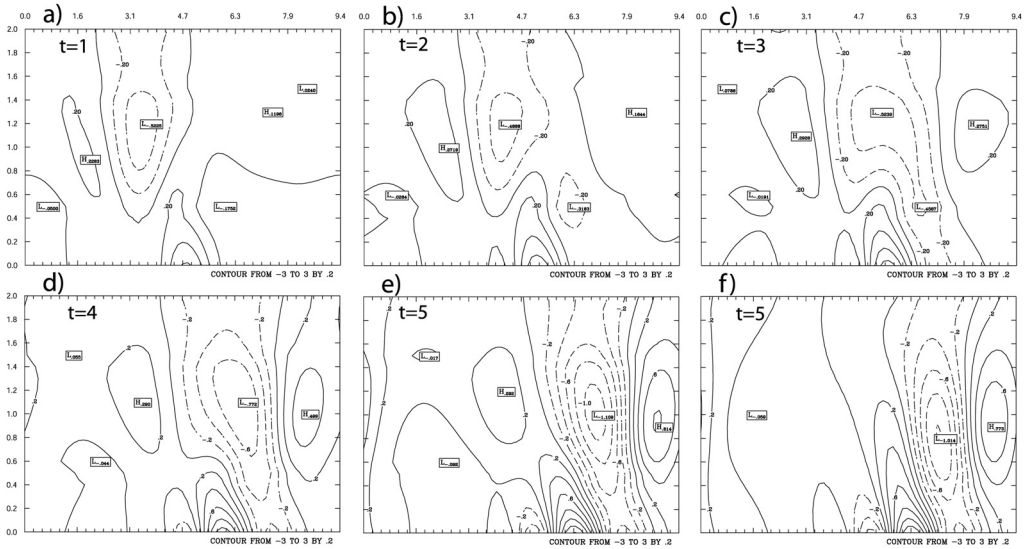

Figure 3. Time sequence of zonal cross-sections at $y = 0$ showing the time evolution of an initial perturbation consisting of a 'cold' monopole plus the deep upper trough for non-dimensional times: (a) 1, (b) 2, (c) 3, (d) 4 and (e) 5; While strong development seems to commence once the upper trough is favourably aligned with the lower feature (between times 3 and 4) the timing is fortuitous. (f) Shows the solution at $t = 5$ when the initial state is only the cold monopole.

and some that are growing or decaying. The dual relative maxima in the vertical and the upstream tilt are characteristic of an unstable normal mode for this flow.

A linear calculation is shown in Fig. 3 in part to simplify the depiction of the structure (since the eddy properties remain centred along $y = 0$). A linear calculation also means the solution evolves by the individual responses of constituent eigenmodes to the mean flow, and no eigenmodes interact. If a similar surface monopole structure were constructed solely from *neutral* eigenmodes, then a linear calculation would have no interaction between the modes. When the initial perturbation includes the upper trough and surface feature that are both constructed from neutral eigenmodes, then the resulting solution only has transient growth or decay by changing superposition as those eigenmodes travel at different speeds. Hence, any growing normal mode seen in the combination plots of Figs. 3(a) to (e) must be a growing normal mode present in the IC, specifically in the analytic cold monopole. That being the case, the combination shown in Fig. 3 is fortuitous. If the initial separation between upper and lower features is greater, a normal-mode-like structure develops ahead of the upper trough. Since the combination in Fig. 3 is fortuitous and does not wait for the surface feature to interact with the upper trough, this is probably not type B cyclogenesis.

If the surface feature can evolve and is constructed solely from neutral eigenmodes, then the only modal interaction in this model arises when nonlinearity is allowed. The interactions being sought are difficult to separate from superposition changes, since both upper and lower features have additional growth or decay initiated by the nonlinearity. To get a robust signal of how the upper feature responds to the lower (but not vice versa), we install one of several analytic, surface-trapped structures into the *prescribed* flow. The prescribed flow, by definition, is mathematically separated from the evolving flow, thus eliminating superposition of the upper trough and the lower feature.

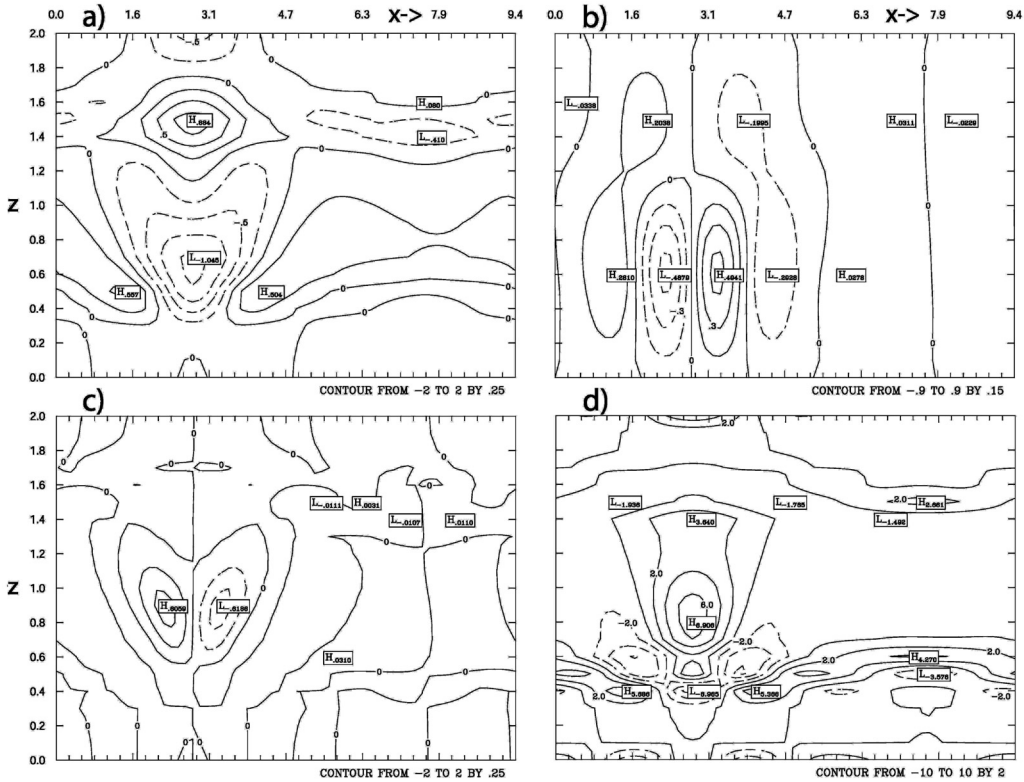

Figure 4. Selected zonal cross-sections at $y = 0.$ and $t = 0.25$ of the deep upper trough which is propagating, nearly neutral, and nearly coherent: (a) temperature field, (b) vertical motion field, (c) baroclinic energy conversion in a quasi-geostrophic total energy equation, and (d) quasi-geostrophic potential vorticity. See text for discussion.

As new eddies appear during the integration, they first appear due east and west of the trough in a linear calculation. In a nonlinear calculation, the leading high tends to be east-north-east, and the trailing high west-south-west, of the initial trough. One might expect this asymmetry when horizontal temperature advection is augmented by the winds of the deep trough. The surface feature also has some impact on eddies that form adjacent to the upper trough. For example, the warm monopole has these mid-troposphere effects—the leading high is drawn northward relative to the upper trough while the trailing high is drawn southward for a *linear* calculation. These motions are consistent with the warm monopole being a low in terms of stream function.

Figure 4 shows additional characteristic properties of the upper trough that explain its relation to the temperature field and how it maintains its shape against the deforming effects of the vertical shear. The deep trough is shown, but the mid8 trough has similar properties. The isolated trough shown in Fig. 1(a) is associated with a cold air pocket in the middle and upper troposphere, and with compensating warm air above; see Fig. 4(a). As the trough moves eastward, it generates vertical motion shown in Fig. 4(b). Ahead of the trough in the upper troposphere and lower stratosphere, the basic flow creates warm advection near the trough and cold advection further east. Differential vorticity advection is small at these levels. Ahead of the trough and in the lower troposphere, vertically increasing vorticity advection exceeds the cold advection so that upward motion is also forced in mid-troposphere. Vertical motion has associated

fields of convergence and divergence. Ahead of the trough, divergence occurs in the upper troposphere and lower stratosphere, whilst convergence occurs in the middle troposphere. Behind the trough is a pattern of opposite sign, making a dipole pattern centred about the trough at any given level. A dipole pattern so centred alters trough propagation. This follows from the QG vorticity equation such that the divergence term opposes the horizontal advection in the upper troposphere and lower stratosphere; in the middle troposphere the divergence term has opposite sign and reinforces the horizontal advection. Without this pattern, the vertical shear in the basic flow would cause the upper trough to develop a tilt to the east with increasing height. Instead, the divergence term, in concert with the horizontal advection, maintains the vertical orientation of the advancing upper-trough axis. Observed developing cyclones have a similar distribution of divergence fields. (Grotjahn (1996b) carries out a similar analysis using the full vorticity equation.) The eddy energetics show a similar compensation to slow down the propagation of the system in the upper troposphere. The rising air ahead of the trough is also relatively cold, and that combination increases the potential energy at the expense of the trough KE. The cold air is also being advected poleward by the motion ahead of the upper trough, and so the baroclinic energy conversion (BCEC; see Fig. 4(c)) is negative ahead of that trough. The strongest negative BCEC is near tropopause level where the mean flow advection of trough energy is also largest. Behind the trough is a compensating positive BCEC; hence BCEC also has a dipole pattern in the upper troposphere. Similar to the vorticity equation analysis, the eddy energy is advected eastward by a vertically sheared basic flow, but that horizontal advection is being slowed down by the BCEC in a way that helps maintain a vertical axis to the eddy energy. The BCEC and divergence fields have zero crossing in the vertical near $z = 0.6$. (Divergence is zero where vertical motion has extrema.) The deep trough, like that shown in Fig. 3, propagates $\sim$1.14 units of distance in 1.7 units of time for an average speed of $\sim$0.7 units; this speed is similar to the basic flow speed at $z = 0.6$ and much less than the 1.1 units basic flow at $z = 0.9$. Finally, since the positive and negative areas of BCEC are nearly equal, the trough is nearly neutral.

Figure 4(d) shows the distribution of QGPV for the upper trough. As one might expect, the primary trough is a positive maximum in QGPV. In the mid to lower troposphere the picture is less clear for the deep trough; additional maxima and minima arise due to ridges adjacent to the main trough at this level and to the rapid decrease of main trough amplitude below $z = 0.5$ (5 km). The mid8 trough has a simpler though similar QGPV distribution with a secondary positive value at the surface.

(*b*) *Cases with no horizontal shear*

'Excess' growth-rate time series (Fig. 5) are used to isolate reactions of the upper feature to favourable alignment with a lower feature. 'Control excess' refers to a growth rate for the combination of deep trough and analytic lower feature shown, minus the growth rate in the control run for the same time, level, and model configuration. Control excess values are shown only for nonlinear runs. The control run has the deep trough but not the lower feature. 'Nonlinear excess' means the nonlinear growth rate minus the linear growth rate for the same combination of upper and lower features. Calculations shown in Fig. 5 have the lower feature in the prescribed state.

When interpreting Fig. 5 it is useful to know when the upper trough reaches key positions relative to the surface-trapped feature. Figures 3(a) to (e) can give some guidance, since the upper trough moves at essentially the same speed in all cases. Figure 3 may be compared with Figs. 2(a) to (c) and Fig. 4 to deduce relative positions of trough properties and surface feature at different times. Specifically, the negative

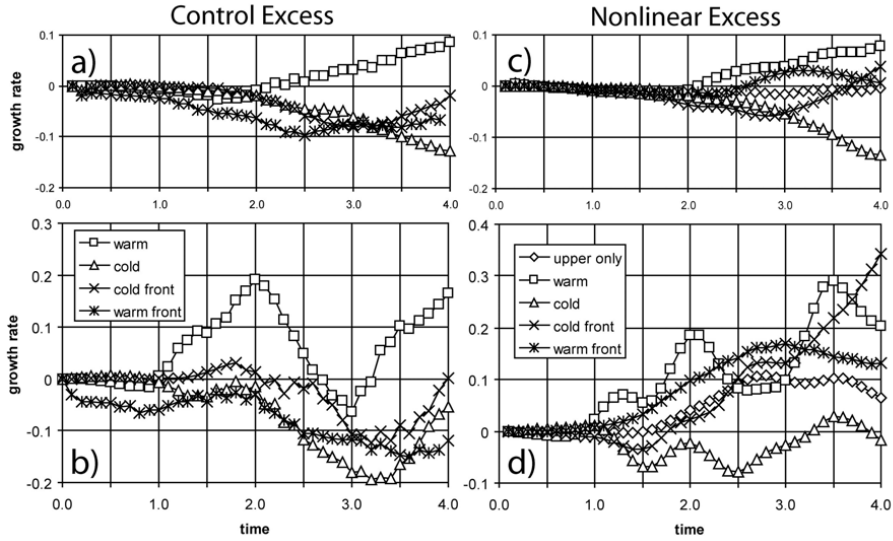

Figure 5. Time series of 'control excess' growth rates of the main trough at two levels, for four different combinations of surface feature and deep upper trough in nonlinear integrations. Control excess growth rates are the actual growth rate minus the growth rate in a control experiment using the deep trough alone; positive values mean that growth exceeds the control case at that time and level. (a) For upper tropospheric level, height $z = 0.9$ near initial maximum in deep initial conditions (IC); (b) lower tropospheric level $z = 0.5$ where the deep IC is small and where the surface-trapped feature reaches zero amplitude; (c) and (d) similar to (a) and (b), respectively, but showing time series of 'nonlinear excess' growth rates (equals nonlinear minus linear growth rate of like kind). The same four surface features are shown, and in addition the nonlinear excess growth rate for the deep trough alone (no surface feature) is indicated as 'upper only'. In the legend 'Warm' refers to the warm monopole, Fig. 2(a); 'cold' is a monopole identical to the warm monopole but opposite in sign; 'cold front' and 'warm front' are as shown in Figs. 2(b) and (c).

BCEC area ahead of the trough (Fig. 4(c)) reaches the west side of the warm (or cold) monopole at time $t \sim 1$. That negative BCEC area is roughly centred over the surface feature at $t \sim 1.9$. The deep trough axis reaches the midpoint of the surface feature at $t \sim 2.8$. The positive BCEC area behind the deep trough is roughly centred over the warm (or cold) monopole at $t \sim 3.7$.

For the upper level (Fig. 5(a)) the growth rates differ little from the control run for the first two units of time. In the control run at level $z = 0.9$ there is a linear change (increasingly negative) in growth rate from 0 at $t = 0$ to -0.05 at $t \sim 2$; then it remains at -0.05 until $t = 3$–3.5. The linear and nonlinear growth-rate time series are very similar in the control run, so this decay is caused by slow dispersion of the components of the deep trough. The difference between nonlinear and linear growth rates is less than 0.02 units magnitude for the control run (see Fig. 5(c) 'upper only' curve). The surface feature has little effect on the upper-tropospheric properties for the deep trough until after two units of time in three of the cases. The exception, the 'warm front', has enhanced decay of the system after $t \sim 1.2$, and most of this is in the linear response. After $t \sim 2$, the warm monopole creates enhanced growth; the cold monopole does the opposite.

At a mid tropospheric level ($z = 0.5$) the deep trough is initially much weaker, and consequently the excess growth rates are larger. Peak magnitudes of 0.2 for control excess growth rates occur for the warm monopole (Fig. 5(b)). Control excess growth rates near 0.2 are about half the value of the most unstable mode in the corresponding linear analysis. The most unstable growth rate for the horizontally uniform basic flow is

0.44 units. The most unstable wave has a longer wavelength than the primary component of the deep trough. So, these growth rates are small, but significant for this model formulation. The control excess growth rates are small or negative for the cold front at this level. The control excess growth rates seen in Fig. 5(b) are negative for the cold monopole and warm front throughout the period.

Nonlinearity adds positively to mid-troposphere growth rates in most cases (the cold anomaly being the exception). In large part this is independent of the surface feature (diamond-shaped points in Fig. 5(d)). Peak values $\sim$0.3 for nonlinear excess growth at $z = 0.5$ occur for the warm monopole and cold front (Fig. 5(d)). The peak value for the cold front occurs later than for the warm monopole. The nonlinear excess growth rates are positive for the warm front, and similar in magnitude but of opposite sign to the control excess rates shown in Fig. 5(b) after $t \sim 1.5$. Hence, nonlinearity approximately halves the negative control excess growth generated by linear terms in the warm-front case. The linear response to the cold front is small but positive between $t \sim 1$ and $t \sim 2$. The nonlinearity first hinders the cold front's effect (nonlinear excess is negative until $t \sim 1.8$) and then enhances growth. The nonlinear excess growth climbs steadily after $t \sim 1.5$ for the cold-front case (Fig. 5(d)). The linear responses to the warm and cold anomalies are slightly enhanced growth. Nonlinearity further enhances the growth for the warm monopole, but reduces it for the cold monopole. These excess growth rates are associated with favourable (or not) orientations between basic properties of the deep trough (Fig. 4) and supplemental motions and energy conversions when a surface feature is introduced. More details are given in the next section.

One may interpret the results using 'PV thinking'. For example, the warm monopole is a trough in the stream function that monotonically decreases as elevation increases. Accordingly, the warm monopole is a shallow, positive maximum in PV. The coherent upper trough has a more complex PV pattern, but a prominent aspect is a positive maximum along the trough axis. Once the upper trough reaches the edge of the low-level warm monopole the lower portion of the trough has enhanced growth. Such growth by PV reinforcement for a zonal displacement of upper and lower PV maxima is well known (e.g. Hoskins *et al.* 1985; Grotjahn 2003). The additional growth caused by the monopole reaches a maximum at $t \sim 2$ units (which is also when the positive BCEC from the monopole most greatly opposes the negative BCEC ahead of the upper trough). At $t \sim 2.8$, the upper trough is directly above the monopole and the two PV maxima no longer amplify each other (and the growth rate is the same as if the warm monopole were not there).

(*c*) *Bickley jet cases*

The deep IC allows comparison with prior work, and is similar to observed cyclone precursors in having little amplitude below 3 km elevation. However, observed cyclones form in a faster flow usually organized into an internal jet. To study a faster jet flow, results are shown for the Bickley jet. The Bickley jet has different eigenfunctions, so a different quasi-coherent, mid8 trough is used (Figs. 1(c) and (d)). The mid8 trough is also used alone and in combination with a variety of surface-trapped features (in the prescribed flow). The mid8 results are broadly consistent with the deep IC results described above, but there are three primary differences. First, the mid8 evolution is much quicker (two to three times faster) in line with the three times greater peak wind speed of the basic flow. Second, the structures that develop from the mid8 IC tend to be much more confined in the meridional direction, in line with how the prominent normal modes have most of their amplitude confined to the vicinity of the prescribed

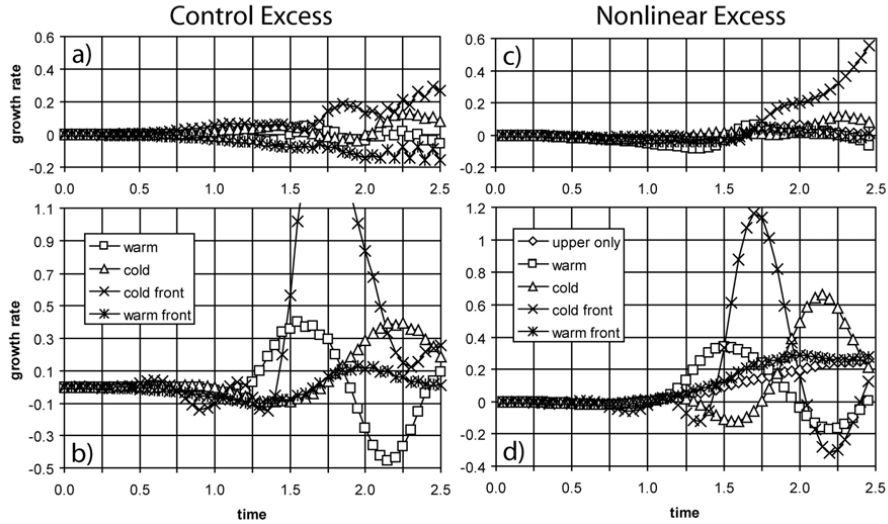

Figure 6. Time series of 'control excess' growth rates for the mid8 trough in a Bickley jet (see text) at two levels for four different combinations of surface feature, where control excess growth rates are the actual growth rate minus the growth rate in a control experiment, for: (a) upper-tropospheric level $z = 0.9$ near initial maximum in mid8 initial conditions (IC); (b) surface level $z = 0$, where mid8 has a weak secondary maximum; (c) and (d) are similar to (a) and (b), respectively, but show time series of 'nonlinear excess' growth rates (equals nonlinear minus linear growth rate of like kind). The same four surface features are shown in each frame with, in addition, the nonlinear excess growth rate for the mid8 trough alone (no surface feature) indicated as 'upper only'. 'Warm' refers to the warm monopole, Fig. 2(d); 'cold' is a monopole identical to the warm monopole but opposite in sign; 'cold front' and 'warm front' are similar to those shown in Fig. 2 for the horizontally uniform basic flow.

flow jet. Third, the quasi-coherent mid8 trough has significant low-level amplitude; this facilitates tracking surface development.

The following properties of the solutions facilitate discussion of the excess growth rates. The upper trough at $z = 0.9$ travels at nearly the same speed in all cases; it overlies the western edge of each surface feature at $t \sim 0.8$ and the centre of the surface feature at $t \sim 1.85$. The most unstable mode for this Bickley jet grows with non-dimensional rate 0.81; this mode has a longer wavelength than the primary components of the initial trough and surface feature in these cases. The stream function axis remains nearly vertical when the surface feature is present. A tilt develops most strongly for the cold-front case, though the tilt is not as great as for a normal mode. The surface feature alters the shape of the low-level trough and adjacent ridges. In most solutions, the trough tends to remain quite close to the initial latitude centred on the Bickley jet with adjacent highs and lows immediately to the east and west. The primary exception is the cold-front case, where the trailing (leading) high forms south (east) of the trough, migrating to the south-west (north-east) of the trough; the trough centre migrates south of the Bickley jet axis. The trough in the lower troposphere for the cold front develops a triangular shape, as growth is enhanced ahead and south-east of the trough (from $t \sim 1$–1.5), primarily where the prescribed surface feature has the pocket of warm air. The low-level trough axis is accelerated south-eastward in the process from $t \sim 1$–2, leading to the greater upstream tilt of the trough axis and location south of the jet noted above. To a lesser degree, a similar asymmetry occurs for the warm monopole case.

Excess growth rates are shown in Fig. 6; as before, the excess growth rates are smaller in the upper troposphere than in the lower troposphere. Surface control experiment excess growth rates are shown in Fig. 6(b). Warm monopole case control

experiment excess peak values are ~0.4 units; as with the no horizontal shear case, the peak values are about half the most unstable normal-mode rate. Control excess growth rates are positive while the upper feature is approaching the warm monopole. A similar orientation has even greater effect for the cold front, where control excess rates peak as the upper feature is over the midpoint of the cold front, where the prescribed surface temperature gradient is largest and with the warm pocket immediately east. Control excess growth rates exceed 1.0 from $t \sim 1.5$–1.9; the largest value exceeds 1.7 at $t = 1.75$. During this time the minimum surface stream function value changes by 5% for the control case, 16% for the warm monopole and 94% for the cold-front case. The cold monopole growth rates are approximately opposite to the warm monopole, being negative as the centre of the monopole is approached and positive after. The warm front has small control excess growth rates.

Nonlinear excess growth rates at the surface (Fig. 6(d)) increase slowly over time when the prescribed surface feature is not present. When surface features are in the prescribed state, the inclusion of nonlinear terms creates similar growth-rate changes as seen for the control excess rates. Again the cold front has very large excess growth rates; the largest value is ~1.2 at $t = 1.75$. The warm monopole enhances growth as the upper trough approaches, then reduces the growth after the trough axis passes over the centre of the monopole. The cold monopole has an opposite pattern to the warm monopole. The nonlinear excess growth is little changed by adding the warm front.

The large excess growth rates of the cold-front case demand additional analysis. The excess growth-rate time series is mirrored in the BCEC. As defined here, the BCEC has advection of the evolving and the prescribed temperature fields by the evolving wind field. The eddy temperature field at the surface is small and positive surrounding the trough. Southerly winds ahead of the quasi-coherent trough cause a net warm advection and positive BCEC. Cold advection trails the trough. Given the warm eddy temperature, the low-level BCEC is negative behind the trough and nearly cancels the positive value ahead. (BCEC at low levels is smaller and of opposite sign to the prominent dipole in Fig. 4(c).) The properties of the prescribed front change the magnitudes of these temperature advections. As the quasi-coherent trough approaches the prescribed cold front, the warm advection is first lessened by the weaker temperature gradient on the cold side of the front and then enhanced on the warm side. The effect is strong enough for the BCEC to have two maxima at $t \sim 0.9$–1.35: one is just west of the trough and the other further east over the prescribed warm sector. After $t \sim 1.35$, the two leading maxima merge. Much of the time after $t \sim 1.3$ the BCEC positive peak exceeds the negative peak by more than 50%. A second factor is the appearance of a cold perturbation in the low-level eddy temperature distribution south-west of the trough. This cold perturbation is consistent both with the enhanced surface high there and the upstream tilt of the trough axis mentioned above. More to the point, the cold perturbation leads to a positive area of BCEC south-west of the trough centre. The negative area of BCEC thus becomes sandwiched between two comparable positive areas after $t \sim 1.9$. These two factors are consistent with the large excess growth rates for the cold-front case.

4. Conclusions

An effort was made to construct combinations of a surface feature and upper trough that approximate the type B growth mechanism in a QG model. Since the description of the type B mechanism has some ambiguity in the original source, the approach has been to test several types of low-level features. The low-level features emphasized include:

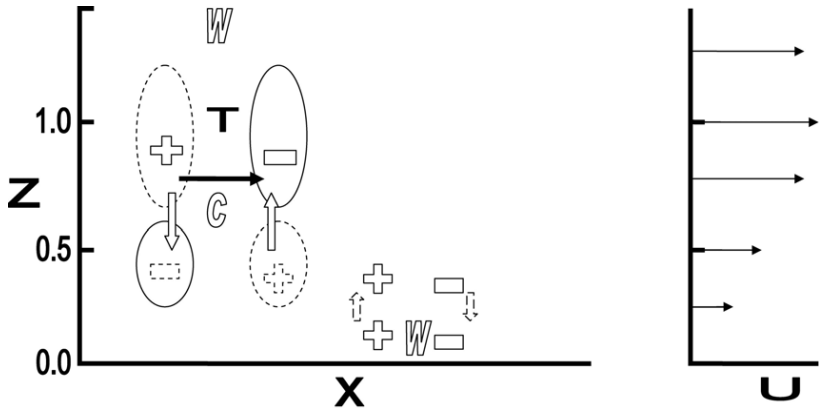

Figure 7. Schematic zonal cross-section showing the vorticity and energy balances for the coherent, isolated, nearly neutral, upper-level trough, with the mean flow (U) as a function of height (z) on the right; z is scaled by 10 km. The deep upper trough is denoted by T and its direction of motion by the solid arrow. The trough has associated temperature variations where C indicates colder air, and W warmer air at the given elevations. Hollow arrows show vertical motions. In the along-flow direction (X) there is upward motion ahead of the trough reaching a maximum near $Z \sim 0.6$. Vertical motion is driven both by temperature advection (from $0.6 < Z < 1.4$) and differential vorticity advection (from $0.3 < Z < 0.7$). Vertical motion has associated divergence (solid oval contours) and convergence (dashed oval contours) fields. From the quasi-geostrophic (QG) vorticity equation, these divergence fields oppose vorticity advection by the mean flow at upper levels, and enhance that advection at lower levels. Therefore, the trough maintains its vertical tilt in the presence of vertical shear. The sign of the baroclinic energy conversion is shown by open + and − signs, and a dashed pattern is used to denote weaker magnitude. The + sign means the time-dependent fields gain energy baroclinically from the prescribed fields. The energy conversion also opposes the mean flow advection of energy similar to the divergence term in the vorticity equation. Also shown are properties generated by the upper trough reacting to a low-level warm anomaly (W in lower right). The low-level anomaly augments vertical motion (dashed arrows), and the baroclinic energy conversion signs (+ and − symbols) are shown.

warm monopole, cold monopole, and two dipolar structures. One dipole approximates a cold front, while the other approximates a warm front. Like observed precursors of cyclogenesis, the upper-level feature is constructed to be nearly coherent, nearly stable, and to maintain a vertical axis while propagating. For those reasons, it has an approximate balance between divergence and convergence, vertical motion, and BCEC ahead of and behind the trough. The upper trough is carefully constructed so that growth is either due to adding nonlinear advection terms or from reaction to a surface-trapped feature or both. The reactions to the surface-trapped features examined exclude superposition of stream function; therefore, growth rates of the stream function value at the centre of the upper trough measure responses to the low-level feature, and not NG by favourable superposition.

The upper feature has properties which are summarized schematically in Fig. 7. Temperature advection and differential vorticity advection lead to rising motion ahead of, and sinking motion behind, the trough. The vertical motion has associated patterns of divergence and convergence. The divergence fields in the QG vorticity equation oppose the horizontal advection of vorticity in the upper troposphere while enhancing the advection in mid troposphere. As a result, the trough axis remains approximately vertical as the trough moves downstream, despite the vertical shear (Fig. 7) of the mean flow. The BCEC pattern is similarly negative ahead and positive behind the trough in the upper troposphere.

A surface feature can affect the development of different parts of the trough in different ways. The growth rate is generally increased as the trough approaches the

warm monopole. The mid-tropospheric portion of the trough may grow by enhancing a region of positive BCEC or by reducing an area of negative BCEC. Sometimes BCEC is enhanced by strengthening equatorward *cold* advection (with strengthened sinking of cold air to adjust eddy potential energy and eddy KE). Hence, the type B growth is not simply growth being established where upward motion occurs above enhanced warm advection associated with enhanced local baroclinicity. (P&S use 'baroclinicity' in at least two different ways; here it is intended to indicate a stronger horizontal temperature gradient.)

The situation is indicated schematically in Fig. 7. When the upper trough first encounters a warm monopole, additional vertical motion and significant BCEC are created in the vicinity of the low-level feature. Figure 7 exaggerates the zonal separation between the upper and lower features in order to isolate the individual patterns associated with each. The warm monopole first increases the mid tropospheric growth when the rising motion west of the warm monopole underlies the rising ahead of the upper trough. The low-level rising air results from southerly winds from the upper trough that advect warm air poleward. The rising cold air ahead of the trough is now moderated by rising warmer air due to the warm monopole, and that reduces the negative BCEC ahead of the trough. The warm monopole is prescribed so it cannot react to the upper trough, and that limits the applicability of this simulation to the type B mechanism. Later stages and other low-level features can be similarly diagnosed.

For example, very large growth rates of the surface feature (doubling-time less than a day) occur when a quasi-coherent trough having significant low-level amplitude encounters a prescribed cold front. The compact warm sector facilitates greatly enhanced BCEC when southerly winds ahead of the trough reach that location. The greatly enhanced BCEC advances the surface feature, and that establishes an upstream tilt with height of the trough. The change of tilt means changes to the temperature field associated with the trough, and that allows positive BCEC to develop behind (as well as ahead of) the trough in the lower troposphere. The horizontal average BCEC increases dramatically, consistent with the large growth rates.

Acknowledgements

The author acknowledges two anonymous reviewers and the editor for encouraging an expanded discussion of the energetics and vertical motion fields. Partial support was provided by NSF grant 0354545.

References

Farrell, B. 1984 Modal and non-modal baroclinic waves. *J. Atmos. Sci.*, **41,** 668–673

Grotjahn, R. 1980 Linearized tropopause dynamics and cyclone development. *J. Atmos. Sci.*, **37,** 2396–2406

1984 Baroclinic instability in a long wave environment. Part II: Ageostrophic energy conversions. *Q. J. R. Meteorol. Soc.*, **110,** 669–693

1996a Composite trough evolution of selected west Pacific extratropical cyclones. *Mon. Weather Rev.*, **124,** 1470–1479

1996b On vorticity equation terms for extratropical cyclones. *Mon. Weather Rev.*, **124,** 2843–2858

2003 'Baroclinic Instability'. Pp. 179–188 in *Encyclopedia of atmospheric sciences*. Volume I. Eds. J. Holton, J. Pyle and J. Curry. Academic Press, Amsterdam, the Netherlands

Grotjahn, R. and Castello, C. 2000 A study of frontal cyclone surface and 300 hPa geostrophic kinetic energy distribution and scale change. *Mon. Weather Rev.*, **128,** 2865–2874

Grotjahn, R., Hodyss, D. and Immel, S. 2003 A technique for creating linearly stable localized atmospheric features with an application to nonlinear cyclogenesis. *Dyn. Atmos. Ocean*, **37,** 25–54

Hakim, G. 2000 Role of nonmodal growth and nonlinearity in cyclogenesis initial-value problems. *J. Atmos. Sci.*, **57,** 2951–2967

Hodyss, D. and Grotjahn, R. 2003 Nonmodal and unstable normal mode baroclinic growth as a function of horizontal scale. *Dyn. Atmos. Ocean*, **37,** 1–24

Hoskins B., McIntyre, M. and Robertson, A. 1985 On the use and significance of potential vorticity maps. *Q. J. R. Meteorol. Soc.*, **111,** 877–946

Mitsudera, H. 1994 Eady solitary waves: A theory of type B cyclogenesis. *J. Atmos. Sci.*, **51,** 3137–3154

Petterssen, S. and Smebye, S. 1971 On the development of extratropical cyclones. *Q. J. R. Meteorol. Soc*., **97,** 457–482

Rotunno, R. and Bao, J.-W. 1996 A case study of cyclogenesis using a model hierarchy. *Mon. Weather. Rev.*, **124,** 1051–1066

Swanson, K. and Pierrehumbert, R. 1994 Nonlinear wave packet evolution on a baroclinically unstable jet. *J. Atmos. Sci.*, **51,** 384–396

Whitaker, J. and Barcilon, A. 1992 Type B cyclogenesis in a zonally varying flow. *J. Atmos. Sci.*, **49,** 1877–1892

US Standard Atmosphere 1976 US Committee on Extension to the Standard Atmosphere. Government Printing Office, Washington, DC, USA